



Thermal analysis and design of a multi-layered rigidity tunable composite



W.L. Shan^{a,*}, T. Lu^a, Z.H. Wang^b, C. Majidi^a

^a Soft Machines Lab, Department of Mechanical Engineering, Carnegie Mellon University, Pittsburgh, PA 15213, USA

^b School of Sustainable Engineering and the Built Environment, Arizona State University, Tempe, AZ 85287, USA

ARTICLE INFO

Article history:

Received 18 April 2013

Received in revised form 8 July 2013

Accepted 9 July 2013

Keywords:

Rigidity tunable composite

Joule heating

Phase change

Low melting-point alloy

Shape memory polymer

Latent heat accumulation

ABSTRACT

Elastomer-based composites embedded with thermally-responsive material (TRM) and a liquid-phase Joule heater are capable of reversibly changing their elastic rigidity by up to four orders of magnitude. At room temperature, the TRM layer is rigid and prevents the surrounding elastomer from elastically bending or stretching. When activated, the embedded Joule heater softens or melts the TRM, which leads to a dramatic reduction in the elastic rigidity of the composite. In this manuscript, we examine the activation of these composites by performing analytical, numerical, and experimental studies of the temperature distribution, thermal history, and phase transition. We consider both low melting point (LMP) metal alloys (e.g. Field's metal) and shape memory polymer (SMP). An analytical solution using the Galerkin Based Integral (GBI) method is derived for the cases where no phase change is involved, while a numerical scheme using the Latent Heat Accumulation (LHA) method is utilized to probe scenarios where phase change has a central role in the elastic rigidity change. The analytical and numerical studies predict a temperature history that is in good agreement with experimental measurements obtained with an IR thermometer. Analysis of the internal temperature distribution leads to scaling laws for determining the required activation time and allowable input power rate for composites containing either LMP alloys or SMP. These scaling laws could potentially be used to inform the design of rigidity tunable composites (RTC) used in assistive wearable technologies and biologically-inspired soft-matter robotics.

© 2013 Elsevier Ltd. All rights reserved.

1. Introduction

Inspired by natural muscle and the catch connective tissue in echinoderms such as sea cucumbers [1], rigidity tunable materials represent an exciting new area in the emerging field of biologically-inspired robotics. These rigidity tunable materials have potential applications in both the military for injury prevention and civilian realms such as wearable robotic assistive devices [2]. Previous efforts for rigidity tunable multifunctional materials include using chemically tuned nano-composite [1], magneto-rheological fluids [3,4], and pneumatic particle jamming [5,6]. While promising for rigidity control in conventional machines and robotics, these methods require external pneumatic, fluidic, and mechanical hardware that may limit their functionality in soft or miniaturized host platforms.

In recent years, engineers have demonstrated reversible elastic rigidity tuning with shape memory polymer-steel laminate composites that are activated with external heating [7,8]. The shape memory polymer exhibits variable stiffness and functions as a connective medium that controls the relative displacement of the rigid

components. At lower temperature the laminate has high flexural rigidity. Upon external heating, however, the SMP softens and allows for translation of the rigid components during deformation. The resulting change in rigidity can be as large as two orders of magnitude. This approach still requires external heating, but the laminate hybrid composite concept opens up new opportunities for design of multifunctional materials with tunable rigidity.

Based on previous efforts, including the recent development of masked deposition techniques for elastically soft electronics [9,10], most recently Shan et al. have fabricated rigidity tunable composites (RTC) with an on-board soft heater [2]. These composites are composed of multiple layers of acrylic VHB tape with low melting point (LPM) metal alloys, such as Field's metal, or with shape memory polymer (SMP). This prototype demonstrates rigidity changes of up to four orders of magnitude [2]. The integrated soft heater component allows the RTC to be used in applications such as wearable assistive devices that require on-board functionality and low power input.

Although promising, the actuation mechanism and underlying physics for RTC technologies with embedded soft-matter heaters has yet to be adequately examined. The presence of phase change and heterogeneity between composite layers presents modeling challenges. There have been recent efforts on analytical and

* Corresponding author. Tel.: +1 732 208 8800.

E-mail addresses: wshan@cmu.edu, wshan@alumni.princeton.edu (W.L. Shan).

Nomenclature

A,B,D,P matrices

a	thermal diffusivity [m^2/s]
b,d,L	dimensions of samples [m]
C_p	specific heat [$\text{J}/\text{kg}/\text{K}$]
\mathbf{d}_n	eigenvectors
$f_i(x)$	basis function
$g(x,t)$	heat source intensity [$\text{J}/\text{m}^3/\text{s}$]
h	heat transfer coefficient [$\text{W}/\text{m}^2/\text{K}$]
I	current [A]
P	power [W]
q	heat flow rate [W]
R	electrical resistance [Ω]
$T(x,t)$	temperature [$^\circ\text{C}$]

Greeks

ℓ	specific latent heat [J/kg]
ρ	density [kg/m^3]
κ	thermal conductivity [$\text{W}/\text{m}/\text{K}$]
γ_n	eigenvalues
$\delta_i, \beta_i, \eta_i$	coefficients
$\theta(x,t)$	differential temperature [$^\circ\text{C}$]

Abbreviations

TRM	thermally-responsive materials
GBI	Galerkin Based Integral
HBI	heat balance integral
SMP	shape memory polymer
LHA	latent heat accumulation
RTC	rigidity tunable composite
LMP	low melting-point

Subscripts

G	Galinstan
V	VHB
F	Field's metal
S	SMP
air	air related variables
g	glass transition temperature
melt	melting point
ef	effective value
e	inclusions, Galinstan, or Field's metal, or SMP

numerical modeling of phase change in 1-D infinite domains [11–15]. There have also been heat diffusion modeling in composites containing heterogeneous materials [16–21]. The combination of these efforts may provide solutions for modeling the current RTC composite design.

Typical analytical approaches to solve a heat diffusion equation include separation of variables, Green's function method, the Heat Balance Integral (HBI) method, and the Galerkin Based Integral (GBI) method [20,22–24]. Here, because of the relatively complex geometry and heterogeneous materials properties, an exact closed-form analytical solution is not readily available. Thus we turn to the integral methods for an approximated solution that is closed-form [22].

The HBI method was first used by von Karman and Pohlhausen to solve boundary-layer problem in fluid mechanics [25]. Goodman then introduced its use in a one dimensional melting problem [26]. Since then this method has found many applications in the solution of one-dimensional heat transfer problems including the one-phase Stefan problem and linear hyperbolic heat-conductions problems on a semi-infinite medium [12–15]. However, these studies cannot be easily extended to a multi-layered problem involving heat generation and phase change within finite domains. The Galerkin based integral method used by Haji-Sheikh et al., which successfully handles heterogeneous material properties [16–18], is more naturally suitable for the problem at hand.

The most popular numerical approaches to one dimensional heat diffusion problems involving phase changes are the enthalpy methods [27–29,11], including many variants such as the apparent heat capacity method [29], and the latent heat accumulation (LHA) method [11]. These methods typically avoid the explicit tracking of the phase change front and thus are easier to implement and require less computational cost. The apparent heat capacity method introduces an enormously large heat capacity over a very small region around the phase change temperature to account for the latent heat absorbed during phase change [11]. The LHA method based on finite volume formulation, however, not only provides the flexibility to track the melting front but also ensures the conservation of energy over the whole domain [11].

In this manuscript, we perform a comprehensive study to examine the activation of RTCs embedded with liquid metal al-

loys and elastomers. The purpose of this paper is to identify the scaling laws that govern the activation times and power requirements for this new class of rigidity-tunable composite. First, an analytical model based on the GBI approach is established and used for rigidity tuning without phase change. Next a one dimensional finite volume numerical model is developed based on the LHA approach to simulate cases involving a constant-temperature melting process. The predicted surface temperature of the composite is then compared with experimental measurements and provides feedback to the numerics. After confirming the validity of the models, temperature profile within the composite are predicted and guidelines on material choice for the RTC are discussed.

2. Material and methods

The RTCs used in this study are made of multiple layers of acrylic elastomer films (VHB™ tapes, 3M™) embedded with a soft-matter Joule heater and layer of thermally-responsive material (TRM). The Joule heater is composed of a serpentine channel of Gallium-Indium alloy (Galinstan; RotoMetals, Inc.) that is liquid at room temperature. Because the heating element is liquid, it can elastically deform with the surrounding material once the composite is activated. The TRM layer may be composed of either a low melting point (LMP) metal alloy (in this study, we used Field's Metal with melting point $T_{\text{melt}} = 62^\circ\text{C}$; RotoMetals, Inc., Fig. 1(a)) or shape memory polymer composites (SMP, Veritex™ with activation temperature $T_g = 62^\circ\text{C}$, Cornerstone Research Group, Inc., Fig. 1(b)).

Details of the rapid fabrication method used to produce these samples are presented in Ref. [2]. In summary, the RTC is composed of two functional components, the Joule heater and the TRM layer (Fig. 1(d)). For the Joule heater, a serpentine channel of Galinstan is deposited on a layer of VHB tape using a laser-patterned mask (30 Watt CO_2 laser engraver; VLS 3.5; Universal Laser Systems, Fig. 1(c)). In the case of Field's metal, the TRM is prepared by depositing melted LMP alloy on a masked layer of VHB tape and then using the double-stick adhesion of the VHB tape to bond it to the Joule heater.

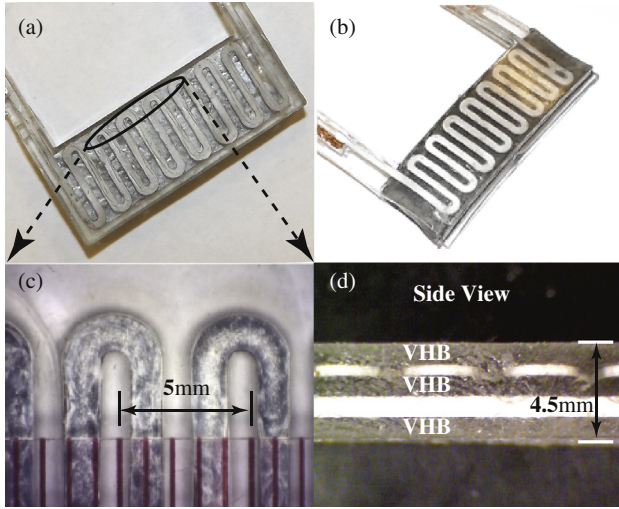


Fig. 1. Rigidity Tunable Composites using (a) Field's metal and (b) shape memory polymer. (c) zoomed-in view of serpentine Galinstan channels of soft heater (d) side view of the RTC sample.

At room temperature, the embedded Field's metal solidifies into a solid strip that prevents the surrounding VHB tape from elastically stretching or bending. When the Joule heater is activated, the Field's metal melts and the elastic rigidity of the composite is governed by the VHB tape, which has an elastic modulus of approximately 128 kPa [2]. This leads to a dramatic reduction in the nominal elastic rigidity of the composite, which is defined as the force required to stretch the composite by a small amount of strain ($\epsilon < 1\%$) divided by the product of strain and the cross-sectional area of the composite.

Referring Fig. 1b, we have also produced RTC samples with SMP. This replacement effectively reduces the rigidity change achievable due to a narrower rigidity change of the SMP itself. However, using SMP eliminates the need to deposit Field's metal at elevated temperatures, further simplifying the fabrication process.

In this study, VHB tapes with two thicknesses, 0.5 mm and 1.0 mm are used. The Galinstan channel is engraved within a $b = 0.5$ mm VHB layer and the channels are 1.27 mm wide and 1.23 mm apart (Fig. 1(c)). The Field's metal or SMP layer of thickness 1.0 mm is embedded within a laser engraved 1.0 mm VHB tape layer. The total thickness of the RTC sample is $9b = 4.5$ mm (Fig. 1(d)), while the width $d = 15$ mm and the length $L = 42$ mm.

2.1. Analytical heat transfer modeling

We examine the thermal activation of the RTC with an analysis that models how the heat generated by the Joule heating elements diffuses through the thickness of the composite. This is accomplished with a transient heat transfer analysis on a simplified one-dimensional representation of the multi-layered composite

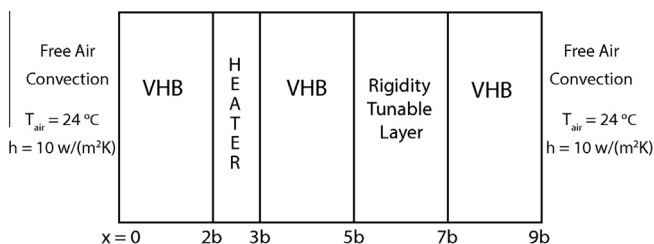


Fig. 2. Schematics of the RTC samples, 1-D simplification through the thickness.

(Fig. 2). By adopting a 1-D model, we assume that the heat loss from the edges of the composite are negligible compared to the heat loss from the top and bottom surfaces.

The governing equation for heat transfer in each layer within the composite is:

$$\kappa(x) \frac{\partial^2 T}{\partial x^2} + g(x, t) = \rho(x) C_p(x) \frac{\partial T}{\partial t}, \quad (x \in [0, 9b]) \quad (1)$$

where $T = T(x, t)$ is the temperature at position x at time t ; $\rho(x) = \rho_i$, $i \in \{V, G, F, S\}$ is the density of the corresponding material, that is, VHB, Galinstan, Field's metal or SMP; similarly, $C_p(x)$ is the specific heat, $\kappa(x)$ is the thermal conductivity, and $g(x, t)$ is the heat source term. Note that we have assumed that the material properties do not change with temperature and time, while they are piecewise continuous in space.

The temperature and the heat flux across the interfaces within the composite are continuous, despite the piecewise continuous material properties. These post additional restraints on the thermal field:

$$\begin{aligned} q_{inter^-} &= q_{inter^+}, \\ T_{inter^-} &= T_{inter^+}. \end{aligned} \quad (2)$$

The heat source term $g(x, t)$ is a nonzero constant in the Galinstan layer as we input constant Joule heating power, which heats up the composite overall. In all other layers, i.e., when $x \in [0, 2b] \cup [3b, 9b]$, the heat source term $g(x, t) = 0$. On the boundaries, the heat loss rate will be determined by free air convection between the composite surfaces and the surrounding environment:

$$\begin{aligned} q|_{x=0} &= h_{air}(T|_{x=0} - T_{air}), \\ q|_{x=9b} &= h_{air}(T|_{x=9b} - T_{air}), \end{aligned} \quad (3)$$

where $q = k \frac{\partial T}{\partial x}|_{x=0,L} \cdot \hat{n}$ is the heat flux out of the top or bottom surface of the RTC sample and \hat{n} is the surface normal, h_{air} is the free air convection heat transfer coefficient for elastomer surface, and T_{air} is the ambient air temperature. In addition, the initial temperature of the sample is at environmental temperature:

$$T(x, 0) = T_{air}. \quad (4)$$

If we define a new variable $\theta(x, t) = T(x, t) - T_{air}$ and assume that the environmental temperature T_{air} is constant, then the governing equation for θ is identical to Eq. (1) while the convective boundary conditions in Eq. (3) and initial temperature in Eq. (4) are all transformed to homogeneous ones:

$$\begin{aligned} \kappa(x) \frac{\partial^2 \theta}{\partial x^2} + g(x, t) &= \rho(x) C_p(x) \frac{\partial \theta}{\partial t}, \quad (x \in [0, L]) \\ \theta_{inter^-} &= \theta_{inter^+}, \\ k_{inter^-} \frac{\partial \theta}{\partial x} |_{inter^-} &= k_{inter^+} \frac{\partial \theta}{\partial x} |_{inter^+}, \\ \left(\frac{\partial \theta}{\partial x} - h_{air} \theta \right) |_{x=0} &= 0, \\ \left(-\frac{\partial \theta}{\partial x} - h_{air} \theta \right) |_{x=L} &= 0, \\ \theta(x, 0) &= 0. \end{aligned} \quad (5)$$

Using the principle of variation of parameters, the solution to the inhomogeneous governing diffusion equation with homogeneous convective boundary conditions and homogeneous initial condition Eq. (5) can be written in the following form:

$$\theta(x, t) = \sum_{n=1}^N c_n(t) F_n(x) \exp(-\gamma_n t), \quad (6)$$

where

$$F_n(x) = \sum_{i=1}^N d_{ni} f_i(x) \tag{7}$$

and $\tilde{\mathbf{d}}_n = (d_{n1}, d_{n2}, \dots, d_{nN})$ is the eigenvector corresponding to eigenvalue γ_n with $f_i(x)$ the basis functions. The values of γ_n and $\tilde{\mathbf{d}}_n$ can be derived from:

$$(\mathbf{A} + \gamma_n \mathbf{B}) \cdot \tilde{\mathbf{d}}_n = 0, \tag{8}$$

in which \mathbf{A} and \mathbf{B} are $N \times N$ matrices with elements in the following form:

$$a_{ij} = \int_0^L f_i \nabla \cdot (k \nabla f_j) dx, \tag{9}$$

$$b_{ij} = \int_0^L \rho C_p f_i f_j dx. \tag{10}$$

The coefficients c_n can be obtained in the following manner [22]:

$$c_n(t) = \sum_{i=1}^N p_{ni} \int_0^t g_i^*(\tau) \exp(\gamma_n \tau) d\tau, \tag{11}$$

where p_{ni} are the elements of $N \times N$ matrix $\mathbf{P} = [(\mathbf{DB})^T]^{-1}$ and $g_i^*(t)$ is defined as follows:

$$g_i^*(t) = \int_0^L g(x, t) f_i(x) dx, \tag{12}$$

where \mathbf{D} is a $N \times N$ matrix with $\tilde{\mathbf{d}}_n$ as its row vectors.

The next step is to find a set of basis functions $f_i(x)$. These are linearly independent polynomial functions that are chosen in a way that they satisfy all of the homogenous boundary conditions. The multi-layered composite can be interpreted as a homogeneous block of VHB elastomer with two inclusions, Galinstan and Field’s metal/SMP, with negligible contact resistance between the layers. In this way, we can obtain the basis functions $f_i(x)$ as polynomials [22]:

$$f_i(x) = (\delta_i x^2 + \beta_i x + \eta_i) x^{i-1}, \tag{13}$$

where δ_i, β_i and η_i are constant coefficients readily available on pp. 319 of Ref. [22].

To accommodate the presence of heterogeneous inclusion, these basis functions need to be modified to be piecewise continuous at the interfaces to allow for continuous temperature and heat flux conditions, as in Eq. (5). Given the layered geometry in the composite, there are two interfaces between each inclusion and the surrounding VHBs. Thus additional polynomials of cubic power are assumed for f_{ie} :

$$f_{ie} = f_i + r_{i1} x^3 + r_{i2} x^2 + r_{i3} x + r_{i4}. \tag{14}$$

Since there are two inclusions, there are eight coefficients r_{jk} corresponding to each basis function. Once the piecewise continuous basis functions are available, the matrices $\mathbf{A}, \mathbf{B}, \mathbf{D}, \mathbf{P}$ and γ_n are all determined accordingly. Finally, the transient temperature during activation of the sample can be expressed as:

$$T(x, t) = T_{air} + \sum_{n=1}^N \left[F_n(x) \exp(-\gamma_n t) \sum_{i=1}^N p_{ni} \int_0^t g_i^*(\tau) \exp(\gamma_n \tau) d\tau \right]. \tag{15}$$

2.2. Numerical heat transfer modeling

The analytical solution derived in last section gives descriptions of both the thermal history at arbitrary position and temperature profile across the sample thickness at arbitrary time. However, with the presence of a first order phase change such as melting,

the extra physics cannot be easily incorporated into the equations and an analytical solution is not readily available. Thus, a one dimensional numerical scheme is also developed to describe the actuation for this scenario.

The heat diffusion governing equation (Eq. (1)) together with boundary conditions (Eq. (3)) and initial conditions (Eq. (4)) is discretized over the finite domain $[0, 9b]$ (the thickness of the RTC sample) using a finite volume method with two-time level schemes [30]:

$$(\rho C_p)_{ef} (T_i - T_i^0) = \frac{\Delta t}{\Delta x} \left[(k_{i+\frac{1}{2}})_{ef} \frac{\alpha(T_{i+1} - T_i) + (1 - \alpha)(T_{i+1}^0 - T_i^0)}{\delta x_{i+\frac{1}{2}}} - (k_{i-\frac{1}{2}})_{ef} \frac{\alpha(T_i - T_{i-1}) + (1 - \alpha)(T_i^0 - T_{i-1}^0)}{\delta x_{i-\frac{1}{2}}} + g_{ef} \Delta x \right]. \tag{16}$$

Here T_i is the temperature at node i of the current time step, T_i^0 is the temperature at node i of the last time step, and $\alpha \in [0, 1]$ is a weighting factor. When $\alpha = 0$, the scheme is explicit; when $\alpha = 1$, the scheme is completely implicit. For values in between, the scheme is partially implicit. Other parameters in a representative control volume are defined in Fig. 3.

On the boundaries where free air convection is assumed, the temperature for the surface nodes are updated at each time step as follows [30]:

$$T_0 = (T_1 + T_{air} h_{air} \Delta x / k_v) / (1 + h_{air} \Delta x / k_v), \tag{17}$$

$$T_N = (T_{N-1} + T_{air} h_{air} \Delta x / k_v) / (1 + h_{air} \Delta x / k_v).$$

To obtain good accuracy in the estimation of the temperature gradient, the control volume has been chosen according to a vertex centered scheme, where every control volume encloses exactly one temperature node and its boundaries are located at the center of two neighboring nodes.

Note that, during the discretization, extra care should be exercised when handling control volumes straddling the interface between heterogeneous materials (Fig. 3). For example, for the VHB-Galinstan interface, $(\rho C_p)_{ef}$ should be the arithmetic mean of the two materials contained; whereas, for the Liquid–Solid Field’s metal interface during melting, $k_{i+\frac{1}{2}, ef}$ should be the harmonic mean of the liquid and solid phase of Field’s metal [30].

The melting of Field’s metal, however, needs extra treatment since it involves additional thermal physics. The metal alloy first absorbs the amount of latent heat before melting begins. Here, we adopted the LHA method, which is described in detail in Ref. [11] and summarized as follows. Essentially, each control volume in the Field’s metal layer is labeled with a phase status and allowed to store an extra amount of heat equal to its latent heat before melting. At each time step, the phase status is first checked. If the nodal phase is ‘Solid’ and its newly computed temperature rises above its melting temperature, the temperature of the node is put back to T_{melt} and the extra heat is put into a depository specially created for this node. The extra heat can be accumulated through the steps. Once it reaches or exceeds the latent heat for this control volume, the label of the phase is changed from ‘Solid’

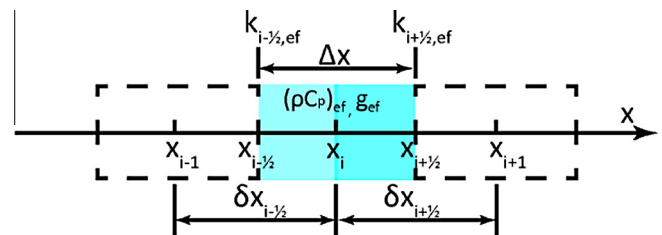


Fig. 3. Representative control volume in simplified 1-D system. Note that the control volume may or may not be homogeneous.

to 'Liquid' and the exceeding part of the extra heat will be reassigned to increase the temperature of the liquid by a corresponding amount. When the phase status is liquid, or is solid but the newly computed temperature is below the melting temperature, the regular heat diffusion equation will be sufficient and the phase status is kept the same.

2.3. Experimental measurements

In addition to the analytical and numerical modeling of thermal actuation within RTC, Joule heating experiments are also conducted by inputting constant current into the RTC samples using a power supply. These samples are in rectangular shape with length $L = 42$ mm and a cross section of width $d = 15$ mm and thickness $9b = 4.5$ mm. For the thermal actuation, constant electrical currents of 6A are used. During the heating process, we record the temperature of the center point of the RTC sample surface close to rigidity tunable component using a Fluke 62 Mini IR thermometer (Fluke Corp. Everett, WA) and a digital camera (Fig. 4). The temperature history of the sample surfaces is then extracted from the video recording. In order to simulate the one dimensional heat diffusion and free air convection boundary conditions in numerics, the samples are suspended in air using four thin strips of VHB (Fig. 4) to minimize heat loss through contact with clamping fixtures.

3. Results

For the analytical approach, 10 basis functions are calculated to ensure accuracy and convergence of the approximated results [16]. Thus 10 sets of $\{\delta_i, \beta_i, \eta_i\}$ and a total of 80 r_{jk} coefficients are calculated to obtain the piecewise continuous basis functions f_i . Adding more basis functions does not show improvement of the results. All of the mathematical calculations are carried out using Mathematica (Version 9; Wolfram Research).

For the numerical approach, both explicit and implicit schemes have been used and no difference is observed in the values obtained for cases where no phase change is involved. Thus the explicit scheme has been used for all the numerical results presented hereafter. The stability requirements on time step and mesh size for explicit numerical scheme are satisfied for all cases as $a\Delta t/\Delta x^2 \leq 0.5$ [30].

For both approaches, we use the material properties presented in Table 1. Note that for those values that are not available in the literature, estimations based on those of similar materials are used.



Fig. 4. Experimental setup for the surface temperature history measurement.

One important property is latent heat for Field's metal, which is initially assumed to be that of Wood's metal. (Table 1).

The surface temperature histories using both the analytical approach and numerical approach for different power inputs have been plotted in Fig. 5. As we can see clearly, the two approaches agree with each other very well before phase change happens. And the presence of melting has greatly increased the activation time for RTC samples using Field's metal. The predicted temperature profiles during heating across the thickness of the sample are also presented in Fig. 6. Again, the results of the two approaches are in good agreement in the sense that the overall temperature profiles are consistent. It should be pointed out that, while the heat flux is continuous on the interfaces for both approaches, the one predicted by the theoretical approach differs from that by the numerical approach. This should be attributed to the nonphysical approximate nature of the theoretical methodology. Notwithstanding these minor discrepancies in heat flux, this comparison serves as a general validation and calibration for the numerical algorithm developed. Also note that these temperature profiles are further validated by comparison between the increased internal energy of the sample and the input energy from Joule heating. Thus, we conclude that these approaches capture the physics of heat transfer reasonably well.

By varying the power input, we fit the temperature history prediction to the experiment results prior to phase change and identified an input power $P = 2.7$ W that can generate similar heating history as measured (Fig. 7,¹ red curve). This value is different from our earlier estimation [2]. The difference may arise from the rough estimate of the electrical resistance of Galinstan channels, with respect to which the power input is very sensitive ($P = I^2R$, $I = 6$ A).

We also observe that the melting process predicted is much longer than experimentally measured (Fig. 7). The difference can be attributed to two possible reasons. First, in the simulation we have taken the latent heat for Wood's metal as that of Field's metal. This value may be too large. Second, we have assumed constant resistance for the Galinstan, ignoring potential thermal effects, which can scale up the true power input as temperature goes up. Here, we focus on the first cause and decrease the latent heat of Field's metal from the value of Wood's metal ($\ell = 39980$ J/kg) to a value ($\ell = 15000$ J/kg) that can give similar temperature history to those measured (Fig. 7, blue curve). We then use this value to probe the thermal limitation of composite functionality during actuation.

4. Discussions

Using the modified latent heat value for Field's metal, we calculate the temperature history during Joule heating at $x = 1$ mm, where the highest temperature resides (Fig. 6) with different power inputs right after the completion of rigidity change (Fig. 8). For a composite composed of Field's metal and VHB, we observe that right after the completion of melting, the highest temperature is close to the upper limit of working temperature for VHB. This limits the activation time for the current design to over 100 s. In order to ensure the functionality of rigidity change, the input power should be carefully regulated, otherwise material failure may occur.

Similar problem exists when Field's metal is replaced by an SMP with a glass transition temperature T_g of 62 °C (Veriflex[®], Cornerstone Research Group, OH). In this case, the benefit of not having latent heat is offset by the extremely low thermal conductivity of SMPs. However, if SMP with 40 °C or lower transition temperature

¹ For interpretation of color in Fig. 7, the reader is referred to the web version of this article.

Table 1
Material properties used for the analytical and numerical modeling of transient heat transfer.

Materials	ρ (kg/m ³)	C_p (J/kg/K)	κ (W/m/K)	ℓ (J/kg)	h_{air} (W/m ² /K)
VHB	960	2010	0.16	–	10
PDMS	970	1460	0.15	–	10
Galinstan	6440	172 ^a	16.5	–	–
Field's Metal (S/L)	9700	172 ^a	31.6 ^a /22.4 ^a	39980 ^a	–
Wax (S/L)	785/749	2140	0.514/0.224	251000	–
SMP (Veritex™)	920 ^b	2400 ^b	0.17 ^b	–	–

^a denotes properties of Wood's metal used instead.
^b denotes the properties of its matrix, Veriflex[®] are used instead.

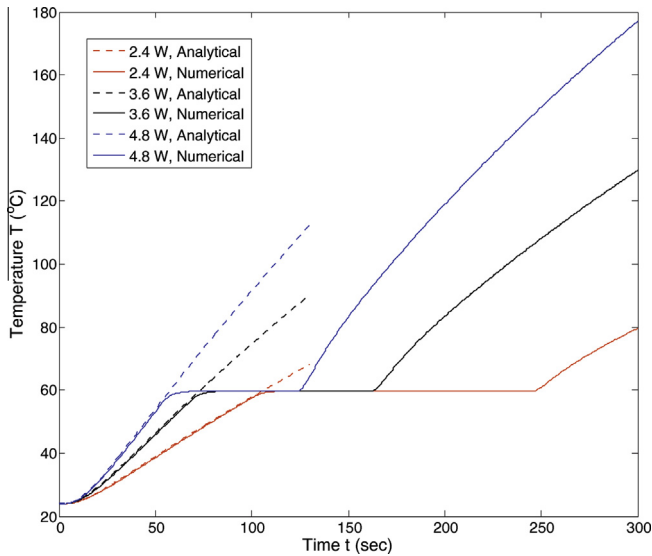


Fig. 5. Surface temperature prediction comparison between analytical modeling and numerical modeling before phase change initiates.

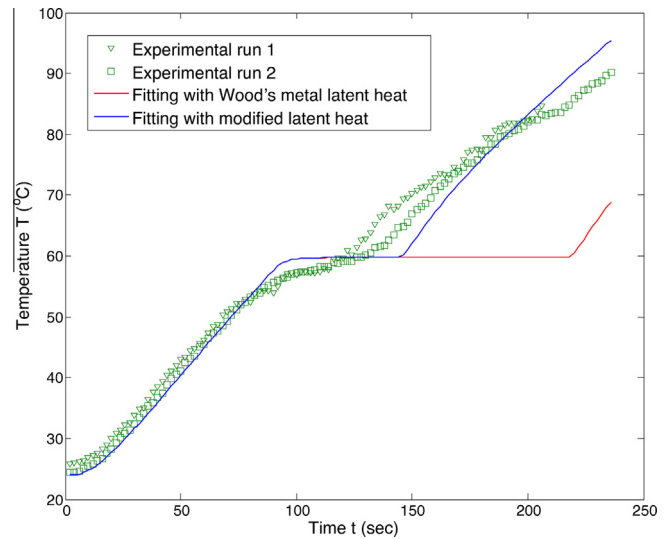


Fig. 7. Numerical prediction of the surface temperature history fitted to the experimental measurements with $P = 2.7$ W.

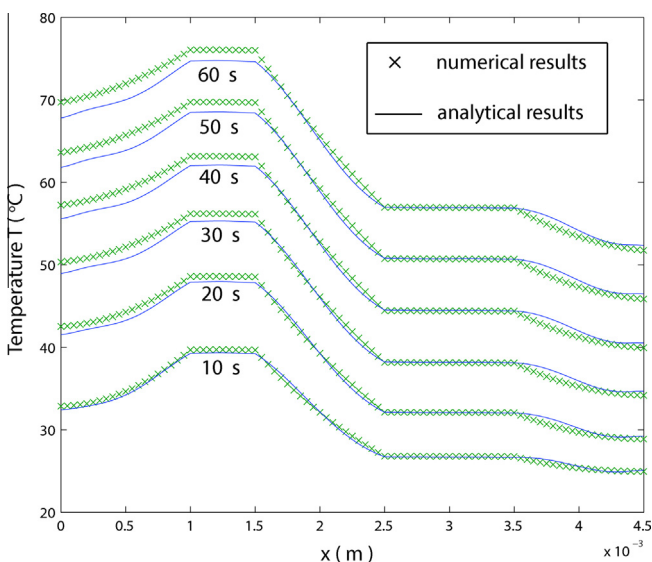


Fig. 6. Predicted temperature profile evolution before phase change by both analytical and numerical modeling. Input power $P = 3.6$ W.

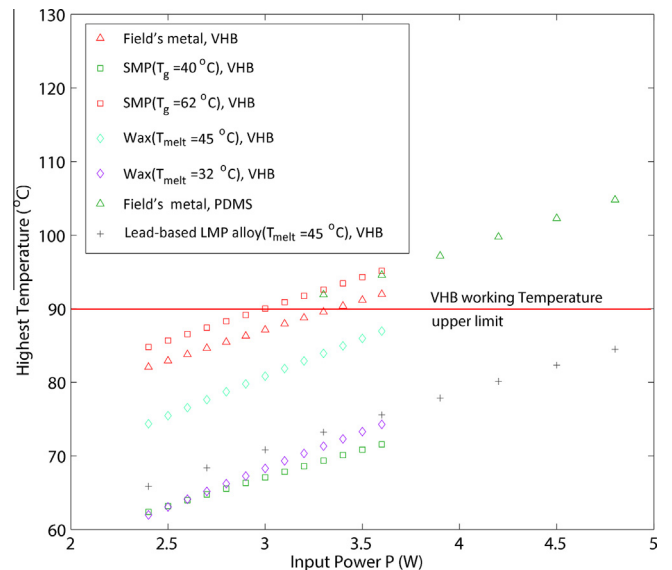


Fig. 8. Highest temperature within composite at completion of rigidity tuning predicted by numerics.

is used, the highest temperature within the composite is fairly below the limit. Thus for the current geometry using SMPs with lower glass transition temperature is a much more reliable design than using Field's metal. Alternatively, for lead-based LMP alloys that have a lower melting temperature of 45 °C, VHB will allow

for significantly great input powers and faster activation times (Fig. 8). We also explore other material choices such as paraffin wax with different melting temperatures. Results show that this could be an excellent choice for composites with VHB as the embedding elastomer. For wax-based composites, the highest tem-

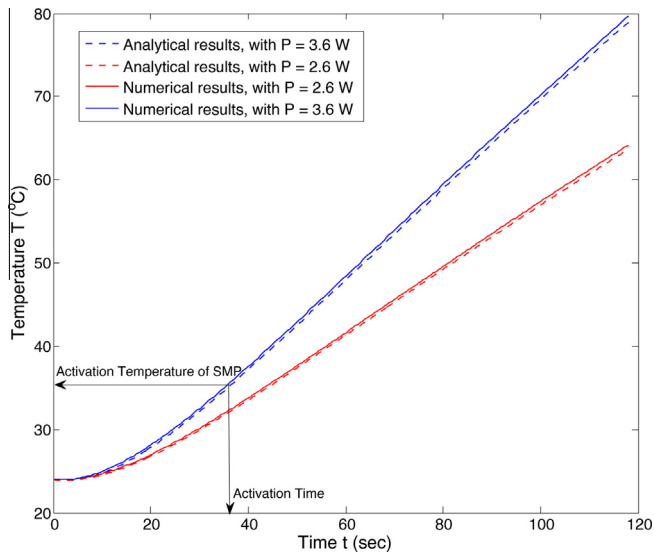


Fig. 9. Predicted activation time of RTC using SMPs with various activation temperature.

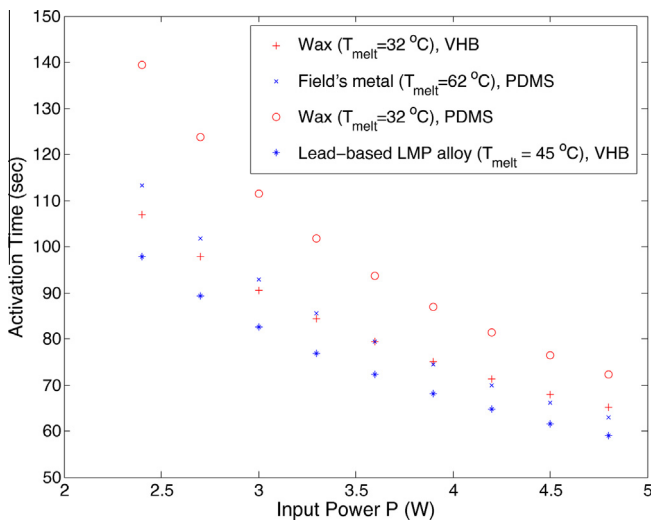


Fig. 10. Predicted activation time of RTC using various thermally responsive materials and elastomers depending on power input.

temperatures is below the upper limit of working temperature of VHB for a large range of input power rates. Notwithstanding the sacrifice in achievable rigidity change, this will also bring other benefits for light-duty devices, considering the comparable density between wax and elastomers.

Another option for bypassing the temperature limitation is to replace VHB with high temperature resistant elastomers such as PDMS, which functions well over 200 °C. The highest temperature predicted using PDMS and Field's metal at completion of rigidity change is also presented in Fig. 8. These results clearly show that the structure will be thermally stable during the rigidity change.

With these models we can also explore the achievable activation time of RTC samples using SMP. Since SMPs with different activation temperatures are available, we expect that the activation time will depend on the glass transition temperatures of SMPs that are shown in Fig. 9. The curves correspond to the thermal history at the edge of the SMP layer furthest away from the heating

source. Points on these curves indicate activation time of composites using SMPs with corresponding glass transition temperature. These predictions suggest the potential for activating RTC samples within 30 s with VHB remaining within its working temperature range.

The achievable activation time dependence on input power and other material choices has also been studied. Fig. 10 presents these dependencies in normal working conditions (P from 2.4 W to 4.8 W). All data indicate a roughly 60 s threshold. Based on these results together with those shown in Fig. 9, in cases where slower activation is allowed and high performance is demanded, PDMS or other similar elastomers with Field's metal is the most appropriate design. If fast activation is prioritized over drastic rigidity change, then SMPs with lower transition temperature and VHB are preferable.

5. Concluding remarks

In this paper we have developed analytical and numerical models along with experimental validation to investigate the actuation of thermally activated rigidity tunable composites. We identify thermally controlled factors that limit the functionality and proposed corresponding solutions to improve the design. We also identify scaling laws that govern the activation times and power requirements for this new class of rigidity-tunable composites. Based on our analysis, we expect to be able to reduce the time necessary to activate SMP-based RTCs to below 30 s. These findings help to inform the design of RTCs composed of elastomers, LMP alloys, SMPs and other TRMs such as paraffin wax.

Acknowledgements

This work was supported by a Defense Advanced Research Projects Agency Young Faculty Award (DARPA YFA #N66001.12.1.4255). The authors thank Prof. A. Haji-Sheikh (University of Texas, Arlington) for helpful discussions on the analytic solution of the thermal analysis.

References

- [1] J.R. Capadona, K. Shanmuganathan, D.J. Tyler, S.J. Rowan, C. Weder, *Science* 319 (2008) 1370–1374.
- [2] W.L. Shan, T. Lu, C. Majidi, *Smart Mater. Struct.* 22 (2013) 085005.
- [3] C. Majidi, R.J. Wood, *Appl. Phys. Lett.* 97 (2010) 164104.
- [4] J.Z. Chen, W.H. Liao, *Smart Mater. Struct.* 19 (2010) 035029.
- [5] V. Trappe, V. Prasad, L. Cipelletti, P.N. Serge, D.A. Weitz, *Nature* 411 (2001) 772–775.
- [6] E. Brown, N. Rodenberg, J. Amend, A. Mozeika, E. Steltz, M.R. Zakin, H. Lipson, H.M. Jaeger, *Proc. Nat. Acad. Sci. USA* 107 (2010) 18809–18814.
- [7] G. McKnight, R. Doty, A. Keefe, G. Herrera, C. Henry, *J. Intell. Mater. Syst. Struct.* 21 (2010) 1783–1793.
- [8] W.W. Clark, J.C. Brigham, C. Mo, S. Joshi, *Proc. SPIE Indust. Commercial Appl. Smart Struct.*, San Diego, CA, 2010, 764507.
- [9] R. Roberts, D.D. Damian, W.L. Shan, T. Lu, C. Majidi, in: *Proc. IEEE Inter. Conf. Robotics and Automation*, Karlsruhe, Germany, 2013, pp. 3514–3519.
- [10] S.H. Jeong, A. Hagman, K. Hjort, M. Jobs, J. Sundqvist, Z. Wu, *Lab on a Chip* 12 (2012) 4657–4664.
- [11] M. Muhieddine, E. Canot, R. March, *Int. J. Finite Volume* 6 (2009) 1–20.
- [12] N. Sadoun, E.K. Si-Ahmed, J. Legrand, *J. Appl. Fluid Mech.* 5 (1) (2012) 105–112.
- [13] S.L. Mitchell, T.G. Myers, *Int. J. Differ. Equ.* 2012 (2012) 187902.
- [14] F.A. Mohamed, *Int. J. Heat Mass Transfer* 33 (1990) 409–416.
- [15] F.A. Mohamed, *Appl. Sci. Res.* 50 (1993) 107–128.
- [16] A. Haji-Sheikh, M. Mashena, *J. Heat Transfer* 109 (1987) 551–556.
- [17] A. Haji-Sheikh, J.V. Beck, *J. Heat Transfer* 112 (1990) 28–34.
- [18] A. Haji-Sheikh, *J. Heat Transfer* 110 (1988) 276–282.
- [19] M. Janicki, G.D. Mey, A. Napieralski, *Microelectron. Reliab.* 42 (2002) 1059–1064.
- [20] Z.H. Wang, S.K. Au, K.H. Tan, *Eng. Struct.* 27 (2005) 1551–1562.
- [21] J. Albers, *IEEE Trans. Compon. Packag. Manuf. Technol.–Part A* 18 (1) (1995) 31–38.
- [22] J.V. Beck, K.D. Cole, A. Haji-Sheikh, B. Litkouhi, *Heat Conduction Using Green's Functions*, Hemisphere Publishing Corporation, 1984.

- [23] H.S. Carslaw, J.C. Jaeger, *Conduction of Heat in Solids*, Oxford: Clarendon Press, 1959.
- [24] K.D. Cole, J.V. Beck, A. Haji-Sheikh, B. Litkouhi, *Heat Conduction Using Green's Functions*, 2nd ed., CRC/Taylor and Francis, 2011.
- [25] H. Schlichting, K. Gersten, *Boundary Layer Theory*, Springer, Berlin, Germany, 2000.
- [26] T.R. Goodman, *Trans. ASME* 80 (1958) 335–342.
- [27] V.R. Voller, M. Cross, *Int. J. Heat Mass Transfer* 24 (1981) 545–556.
- [28] V.R. Voller, M. Cross, N.C. Markatos, *Int. J. Numer. Meth. Eng.* 24 (1987) 184–271.
- [29] C. Bonacina, G. Comini, A. Fasano, M. Primicerio, *Int. J. Heat Mass Transfer* 16 (1973) 1825–1832.
- [30] W. Tao, *Numerical Heat Transfer*, 2nd ed., Xi'an Jiaotong University Press, Xi'an, China, 2001.